Supporting Information

Mesoporous $MnCo_2O_4$, $NiCo_2O_4$, and $ZnCo_2O_4$ Thin Film Electrodes as Electrocatalysts for Oxygen Evolution Reaction in Alkaline Solutions

Assel Amirzhanova,[1] Nesibe Akmanşen,[1] Irmak Karakaya,[1] and Ömer Dag[1,2]*

[1]Department of Chemistry, Bilkent University, 06800, Ankara, Turkey.

[2] UNAM — National Nanotechnology Research Center and Institute of Materials Science and Nanotechnology, Bilkent University, 06800, Ankara, Turkey.

Email: dag@fen.bilkent.edu.tr

Table S1. List of chemicals used in all solutions and mesoporous films.

Salts/Surfactant (Mole Ratio)	**$[Ni(H_2O)_6](NO_3)_2$ (mg)**	**$[Co(H_2O)_6](NO_3)_2$ (mg)**	**$C_{12}E_{10}$ (mg)**	**CTAB (mg)**	**Ethanol (ml)**
6	464	929	500	291	5
8	629	1239	500	291	5
10	774	1548	500	291	5
12	928	1858	500	291	5
15	1160	2322	500	291	10
20	1547	3097	500	291	10
25	1934	3871	500	291	10
Salts/Surfactant (Mole Ratio)	**$[Ni(H_2O)_6](NO_3)_2$ (mg)**	**$[Co(H_2O)_6](NO_3)_2$ (mg)**	**P123 (mg)**	**CTAB (mg)**	**Water (ml)**
60	500	989	500	314	5
Salts/Surfactant (Mole Ratio)	**$[Mn(H_2O)_4](NO_3)_2$ (mg)**	**$[Co(H_2O)_6](NO_3)_2$ (mg)**	**$C_{12}E_{10}$ (mg)**	**CTAB (mg)**	**Ethanol (ml)**
6	401	929	500	291	5
8	535	1239	500	291	5
10	669	1548	500	291	5
12	803	1858	500	291	5
15	1004	2322	500	291	10
20	1339	3097	500	291	10
25	1673	3871	500	291	10
Salts/Surfactant (Mole Ratio)	**$[Zn(H_2O)_6](NO_3)_2$ (mg)**	**$[Co(H_2O)_6](NO_3)_2$ (mg)**	**P123 (mg)**	**CTAB (mg)**	**Water (ml)**
30	512	1000	1000	341	5
60	1024	2000	1000	341	5
90	1536	3000	1000	341	5

Table S2. Electrochemical parameters for OER of common spinel transition metal oxides.

Catalyst	Electrolyte	Substrate	Overpotential at 1 mA/cm^2 (mV)	Overpotential at 10 mA/cm^2 (mV)	Tafel Slope (mV/dec)	Reference
RuO_2	1 M NaOH	Carbon Paper		273	48.3	[1]
IrO_2	1 M NaOH	Carbon Paper		310	52 ± 2	[1]
$NiCo_2O_4$	1 M NaOH	Carbon Paper		381	74	[1]
$NiCo_2O_4$	1 M NaOH	FTO		340	51	[2]
$ZnCo_2O_4$	1 M KOH	Pt	260	400	47	[3]
Co_3O_4	1 M KOH	Pt	320	420	54	[3]
$MnCo_2O_4$	1 M KOH	GCE		507	94	[4]
$MnCo_2O_4$	0.1 M KOH O_2-saturated	GCE		400	90	[5]
Mn_3O_4	1 M KOH	Ni foam		287	86	[6]
$CuCo_2O_4$	1 M KOH	Ni foam			117	[7]
$CoFe_2O_4$	0.1 M KOH	GCE			82	[8]
$MnFe_2O_4$	0.1 M KOH	GCE			114	[8]
$CuFe_2O_4$	0.1 M KOH	GCE			94	[8]
$NiFe_2O_4$	1 M KOH	nickel foam		267	36.7	[9]
$CoCr_2O_4$	1 M KOH	GCE		422	63.3	[10]
$MnCo_2O_4$	**1 M KOH**	**FTO**	**241**	**440**	**75**	**This work**
$NiCo_2O_4$	**1 M KOH**	**FTO**	**215**	**404**	**59**	**This work**
$ZnCo_2O_4$	**1 M KOH**	**FTO**	**264**	**430**	**54**	**This work**

References

(1) Li, J.; Chu, D.; Dong, H.; Baker, D. R.; Jiang, R. Boosted oxygen evolution reactivity by igniting double exchange interaction in spinel oxides. *J. Am. Chem. Soc.* **2020**, *142*, 50–54.

(2) Wang, H. Y.; Hsu, Y. Y.; Chen, R.; Chan, T. S.; Chen, H. M.; Liu, B. Ni^{3+}-Induced formation of active NiOOH on the spinel Ni-Co oxide surface for efficient oxygen evolution reaction. *Adv. Energy Mater.* **2015**, *5*, 1500091.

(3) Kim, T. W.; Woo, M. A.; Regis, M.; Choi, K. S. Electrochemical synthesis of spinel type $ZnCo_2O_4$ electrodes for use as oxygen evolution reaction catalysts. *J. Phys. Chem. Lett.* **2014**, *5*, 2370–2374.

(4) Rani, B. J.; Yuvakkumar, R.; Ravi, G.; Hong, S. I.; Velauthapillai, D.; Guduru, R. K.; Thambidurai, M.; Dang, C.; Al-Onazi, W. A.; Al-Mohaimeed, A. M. Electrochemical water splitting exploration of $MnCo_2O_4$, $NiCo_2O_4$ cobaltites. *New J. Chem.* **2020**, *44*, 17679–17692.

(5) Wang, W.; Kuai, L.; Cao, W.; Huttula, M.; Ollikkala, S.; Ahopelto, T.; Honkanen, A. P.; Huotari, S.; Yu, M.; Geng, B. Mass-production of mesoporous $MnCo_2O_4$ spinels with manganese(IV)- and cobalt(II)-rich surfaces for superior bifunctional oxygen electrocatalysis. *Angew. Chem. Int. Ed.* **2017**, *56*, 14977–14981.

(6) Yu, M. Q.; Li, Y. H.; Yang, S.; Liu, P. F.; Pan, L. F.; Zhang, L.; Yang, H. G. Mn_3O_4 nano-octahedrons on Ni foam as an efficient three-dimensional oxygen evolution electrocatalyst. *J. Mater. Chem. A* **2015**, *3*, 14101–14104.

(7) Aqueel Ahmed, A. T.; Hou, B.; Chavan, H. S.; Jo, Y.; Cho, S.; Kim, J.; Pawar, S. M.; Cha, S. N.; Inamdar, A. I.; Kim, H.; Im, H. Self-assembled nanostructured $CuCo_2O_4$ for electrochemical energy storage and the oxygen evolution reaction via morphology engineering. *Small* **2018**, *14*, 1800742.

(8) Li, M.; Xiong, Y.; Liu, X.; Bo, X.; Zhang, Y.; Han, C.; Guo, L. Facile synthesis of electrospun MFe_2O_4 (M = Co, Ni, Cu, Mn) spinel nanofibers with excellent electrocatalytic properties for oxygen evolution and hydrogen peroxide reduction. *Nanoscale* **2015**, *7*, 8920–8930.

(9) Liu, J.; Zhu, D.; Ling, T.; Vasileff, A.; Qiao, S. Z. S-$NiFe_2O_4$ Ultra-small nanoparticle built nanosheets for efficient water splitting in alkaline and neutral pH. *Nano Energy* **2017**, *40*, 264–273.

(10) Al-Mamun, M.; Su, X.; Zhang, H.; Yin, H.; Liu, P.; Yang, H.; Wang, D.; Tang, Z.; Wang, Y.; Zhao, H. Strongly coupled $CoCr_2O_4$/Carbon nanosheets as high performance electrocatalysts for oxygen evolution reaction. *Small* **2016**, *12*, 2866–2871.

Table S3. Faradaic efficiency data.

Electrode	Time (Min)	Theoretical O_2 (µmol)	Experimental O_2 (µmol)	Faradaic Efficiecy (%)
m-$NiCo_2O_4$-350	10	17.98	18.25	65.2
m-$NiCo_2O_4$-350	30	90.29	83.19	92.1
m-$MnCo_2O_4$-350	10	13.89	13.00	93.6
m-$MnCo_2O_4$-350	30	47.62	40.91	85.9
m-$ZnCo_2O_4$-350	10	26.87	13.74	51.1
m-$ZnCo_2O_4$-350	30	84.83	61.89	73.0

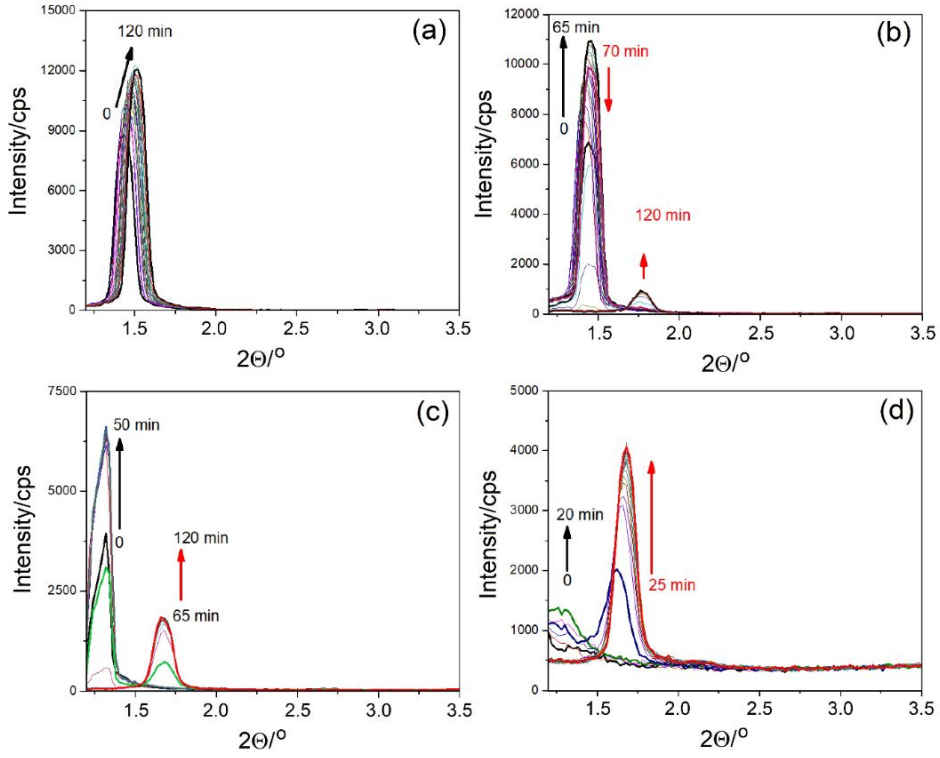

Figure S1. Aging of fresh films: Small angle XRD pattern of (a) MnCo-6, (b) MnCo-8, (c) MnCo-10, and (d) MnCo-12.

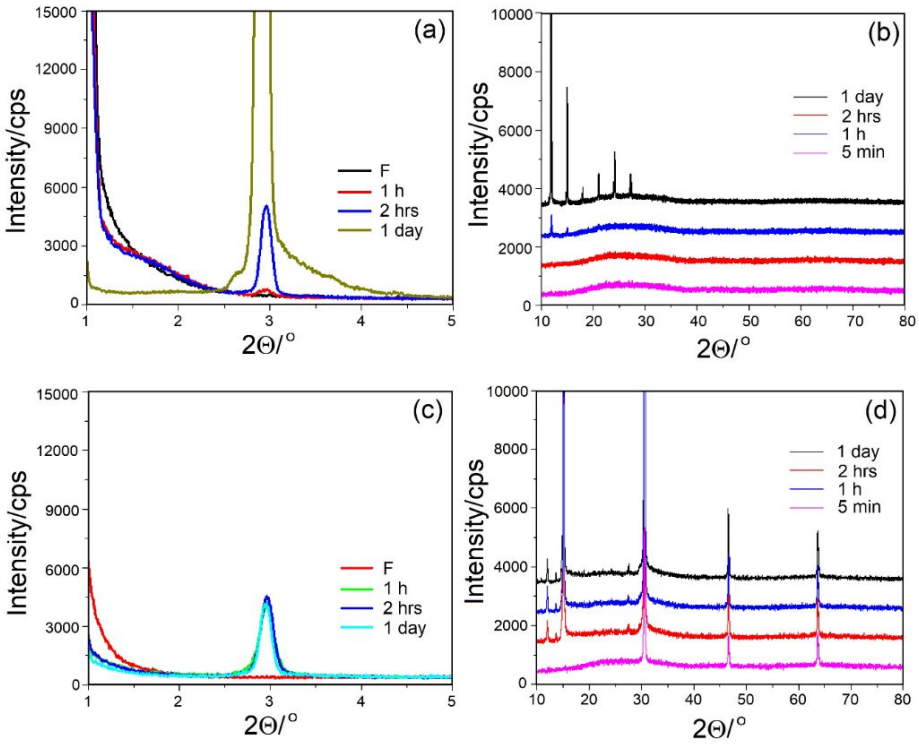

Figure S2. Small and wide angle XRD patterns of ZnCo-# gel phases, recorded during aging process, where # is (a and b) 30 and (c and d) 60.

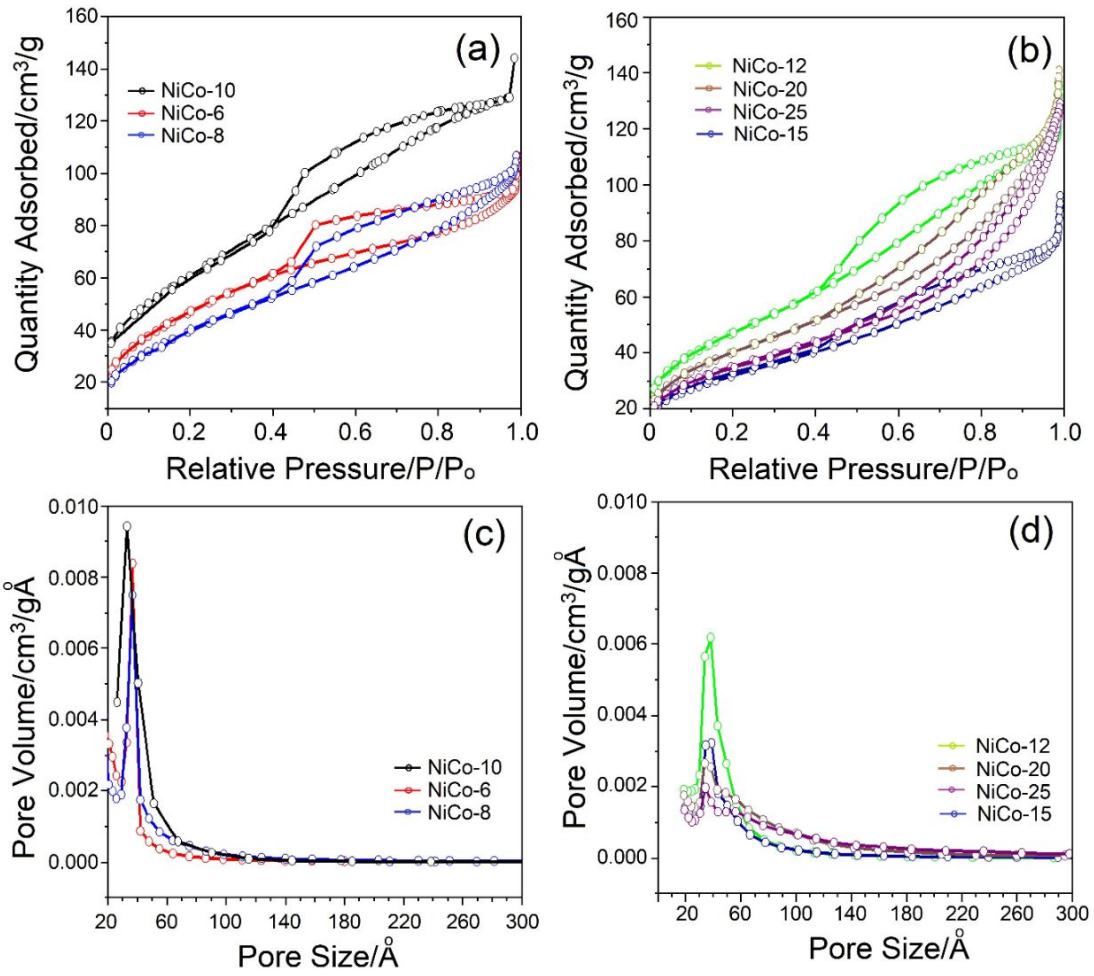

Figure S3. (a and b) N_2(77 K) adsorption-desorption isotherms and (c and d) pore size distribution plots of m-$NiCo_2O_4$-#-250 (# is indicated in the plots).

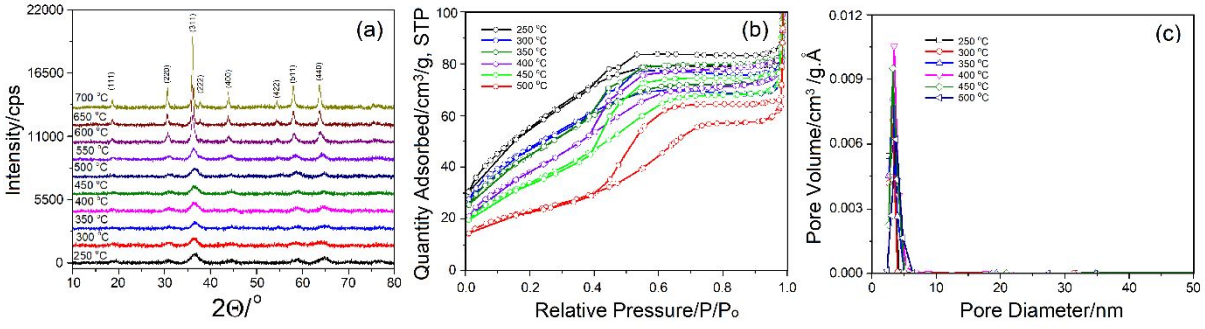

Figure S4. m-$MnCo_2O_4$ (calcined at indicated temperatures): (a) PXRD patterns (indexed using PDF card no: 00-023-1237), (b) N_2 adsorption-desorption isotherms, and (c) pore-size distribution plots.

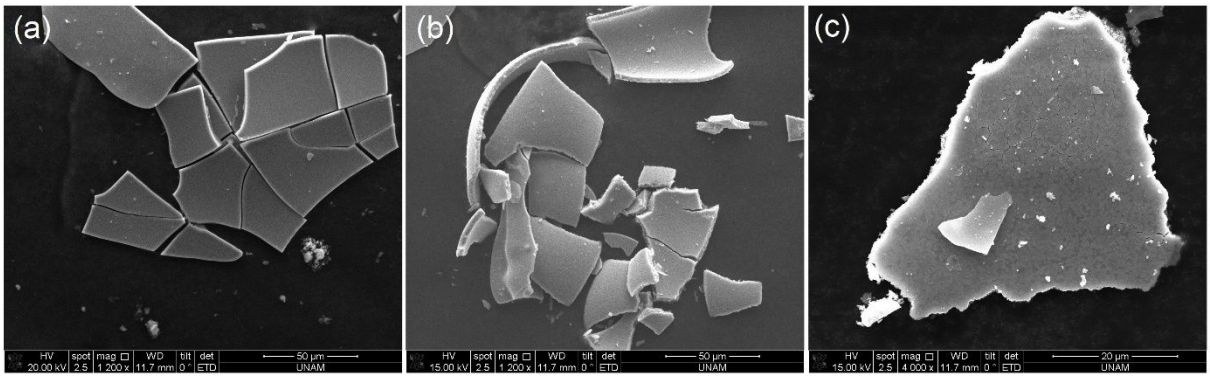

Figure S5. SEM images of m-$MnCo_2O_4$-n-300 with n of (a) 10, (b) 15, and (c) 25.

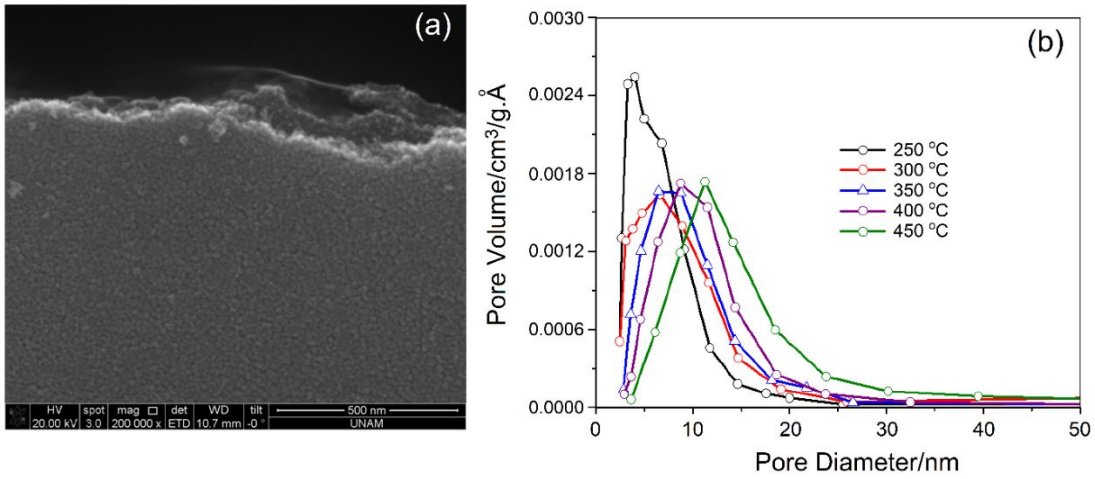

Figure S6. (a) SEM image of m-$ZnCo_2O_4$ and (b) pore size distribution plots of m-$ZnCo_2O_4$-60, calcined at 250 °C and annealed at indicated temperatures.

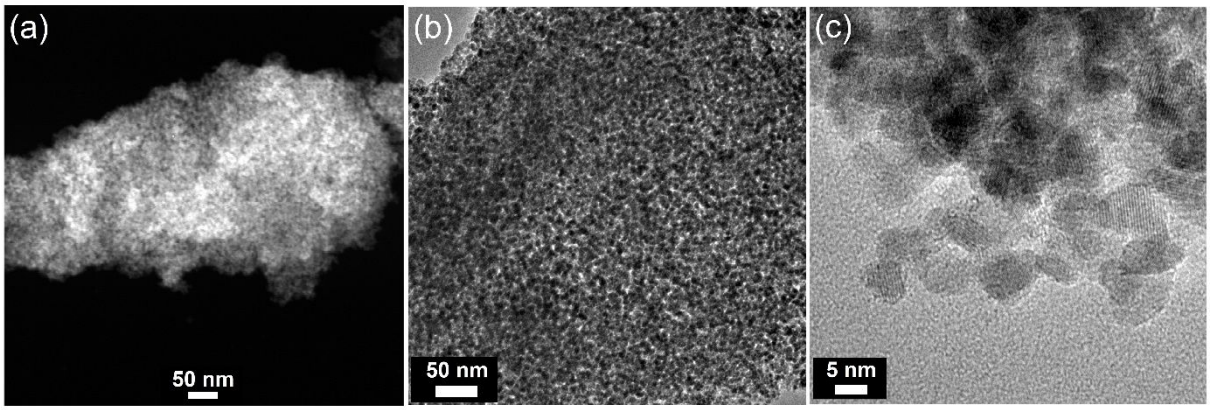

Figure S7. (a) HAADF and (b and c) TEM images of m-$ZnCo_2O_4$-60-350.

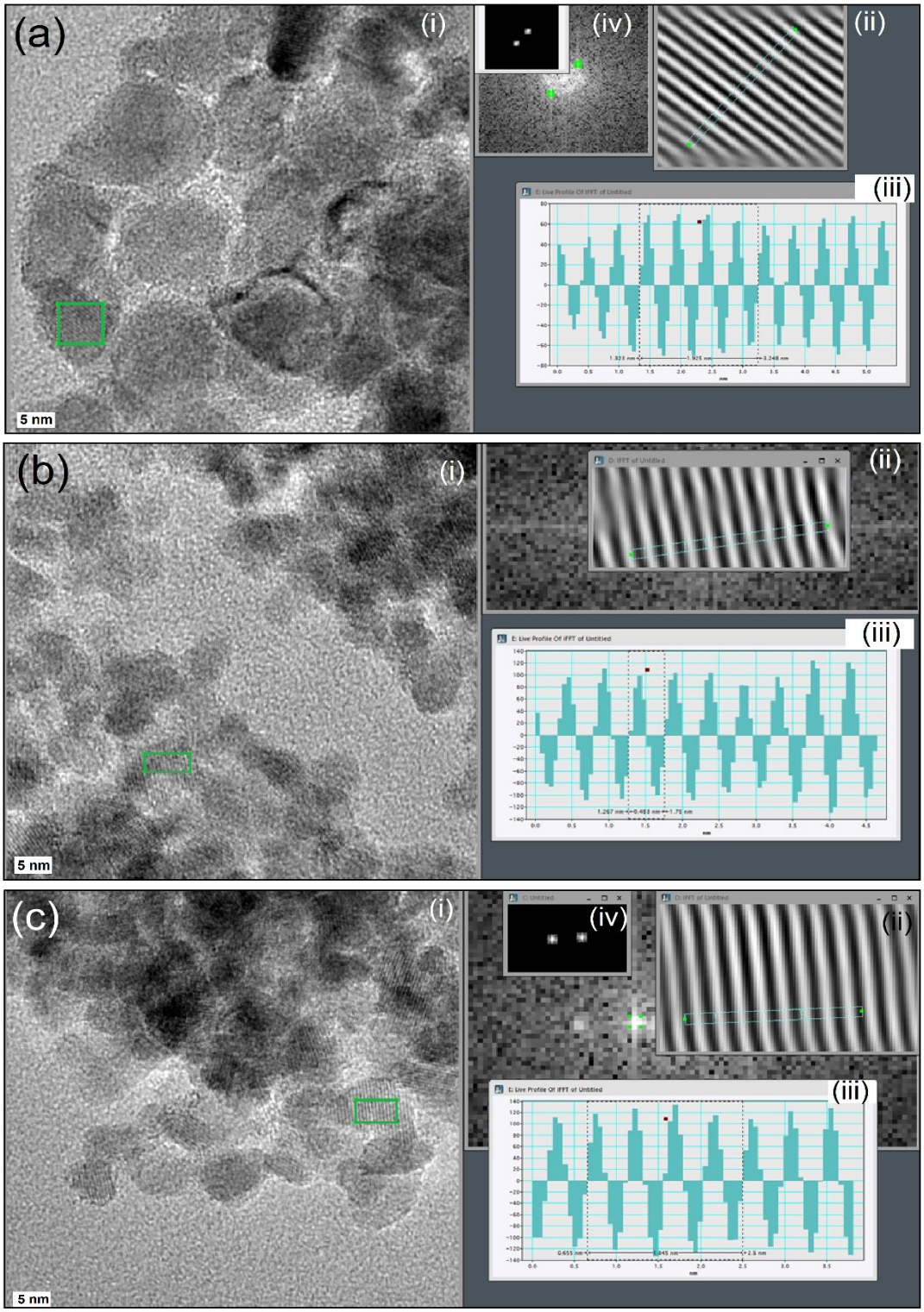

Figure S8. HR-TEM images and analysis of the samples calcined at 350 °C: (i) TEM images, (ii) back FFT of the selected areas in green squares and rectangles (iii) histograms along the lines in panels (ii) and (iv) FFTs of the same selected areas in panels (i) of (a) m-$NiCo_2O_4$, (b) m-$MnCo_2O_4$, and (c) m-$ZnCo_2O_4$.

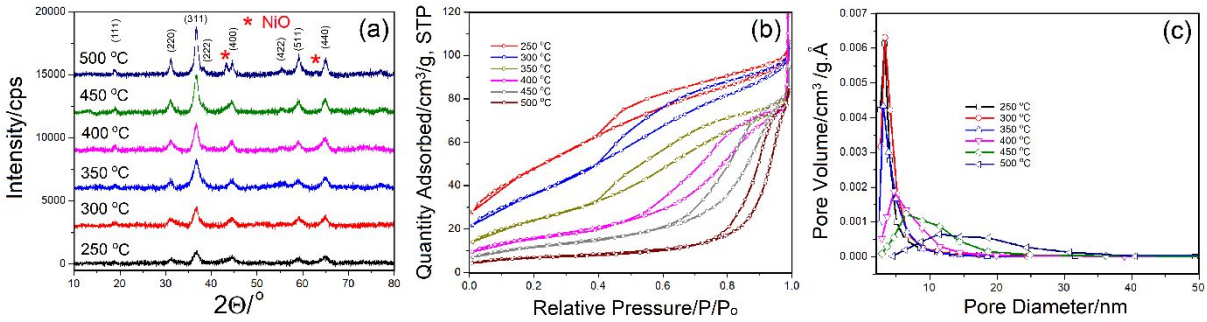

Figure S9. m-$NiCo_2O_4$-60-XXX (XXX are indicated over the plots with color coding). (a) XRD patterns, (b) (77 K) N_2 adsorption-desorption isotherms, and (c) pore size distribution plots.

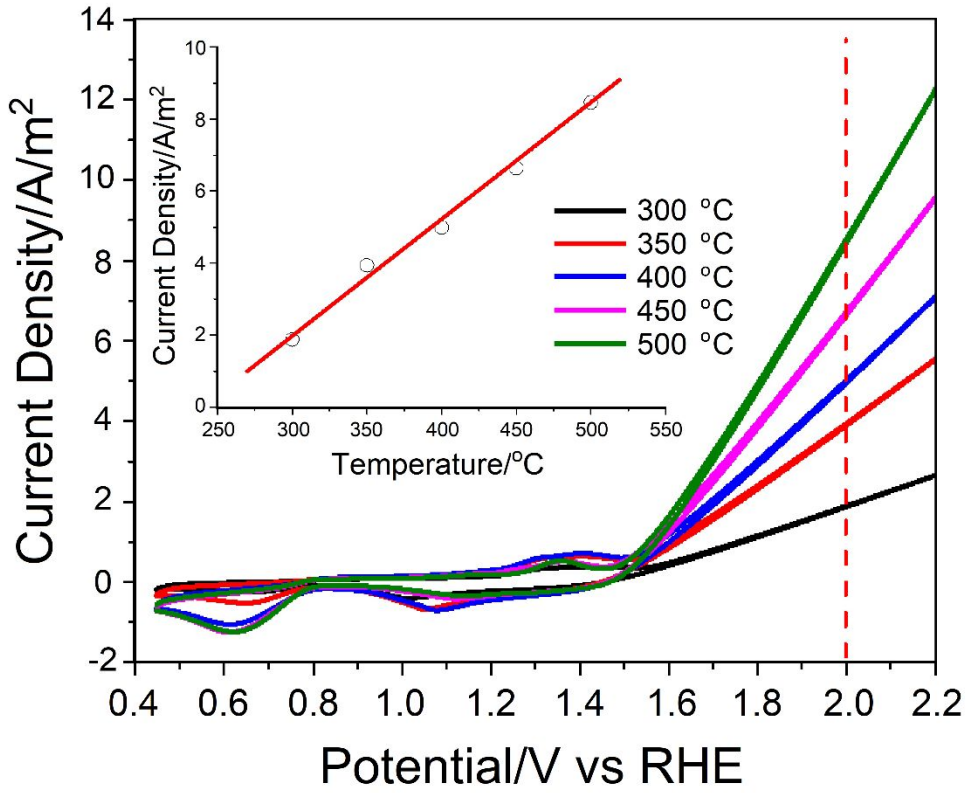

Figure S10. Normalized CVs of m-$NiCo_2O_4$-10-XXX (XXX are given in the plot) with respect to actual surface area of the electrodes (inset is plot of current density at 1.0 versus annealing temperatures).

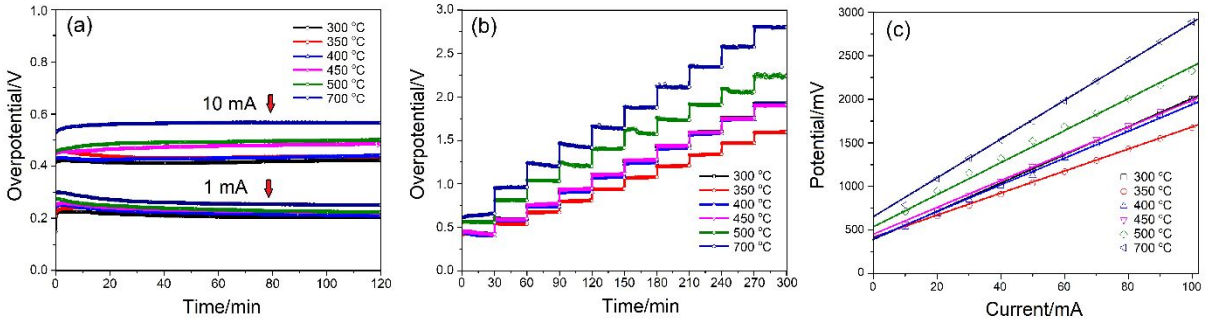

Figure S11. m-$NiCo_2O_4$-10 electrodes: (a) CP plots of m-$NiCo_2O_4$-10 at 1 (bottom set) and 10 mA/cm^2 current densities (top set) and (b) multistep CP plots from 10 to 100 mA/cm^2 current densities with 10 mA increments. (c) Potential versus current plots from multistep CPs of m-$NiCo_2O_4$-10-XXX (XXX values are calcination temperature as indicated in the plots).

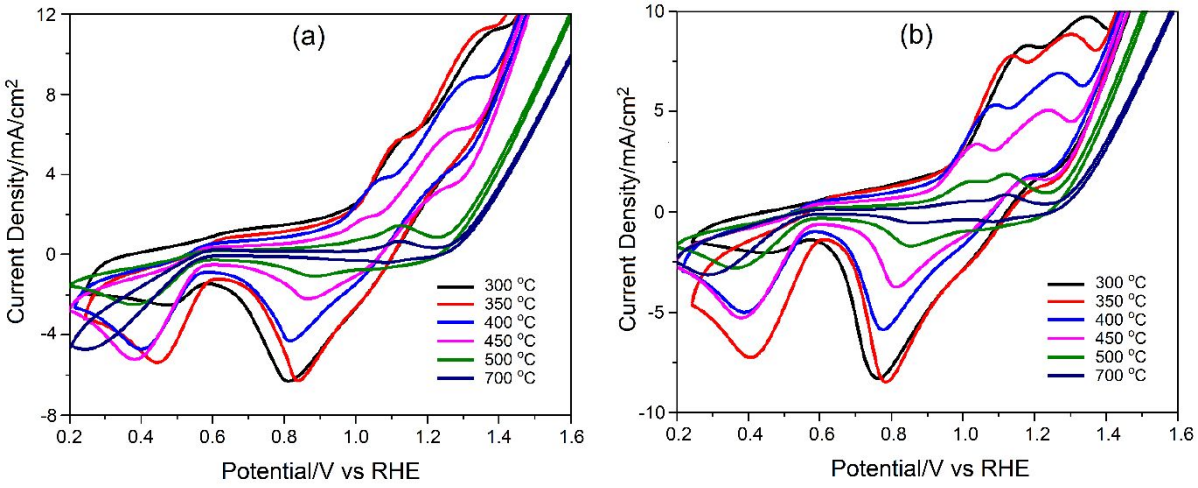

Figure S12. CVs before (a) and after (b) multi step CP experiments of m-$NiCo_2O_4$-10-XXX (XXX values are given in the color codes).

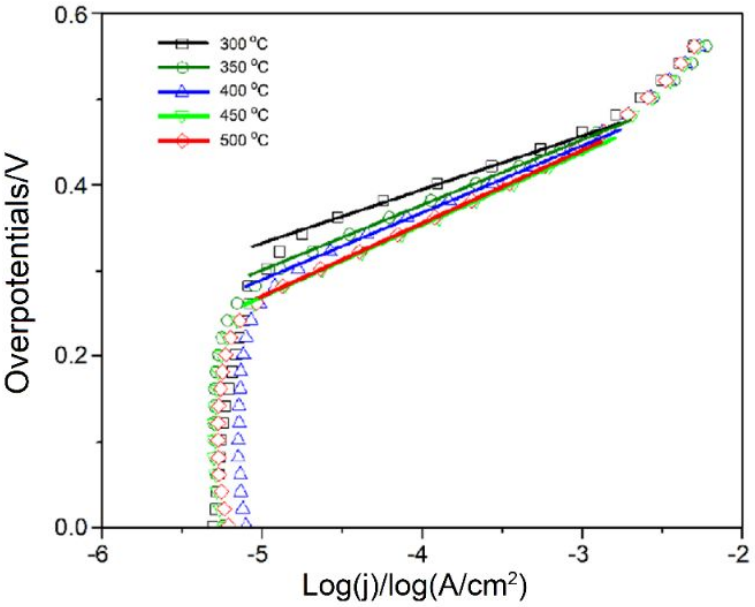

Figure S13. Tafel plots of m-$MnCo_2O_4$-10-XXX (XXX are given in the plots).

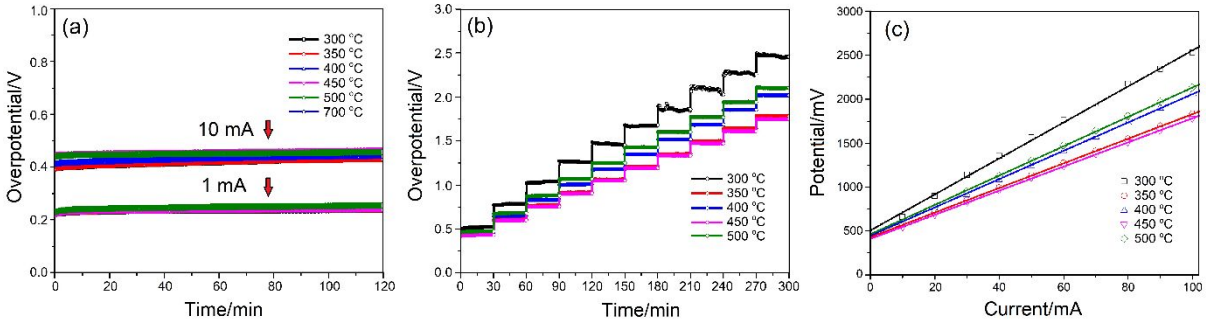

Figure S14. m-$MnCo_2O_4$-10 electrodes: (a) CP plots of at 1 (bottom set) and 10 mA/cm^2 current densities (top set) and (b) multistep CP plots from 10 to 100 mA/cm^2 current densities with 10 mA increments. (c) Potential versus current plots from multistep CPs of m-$MnCo_2O_4$-10-XXX (XXX values are calcination temperature as indicated in the plots).

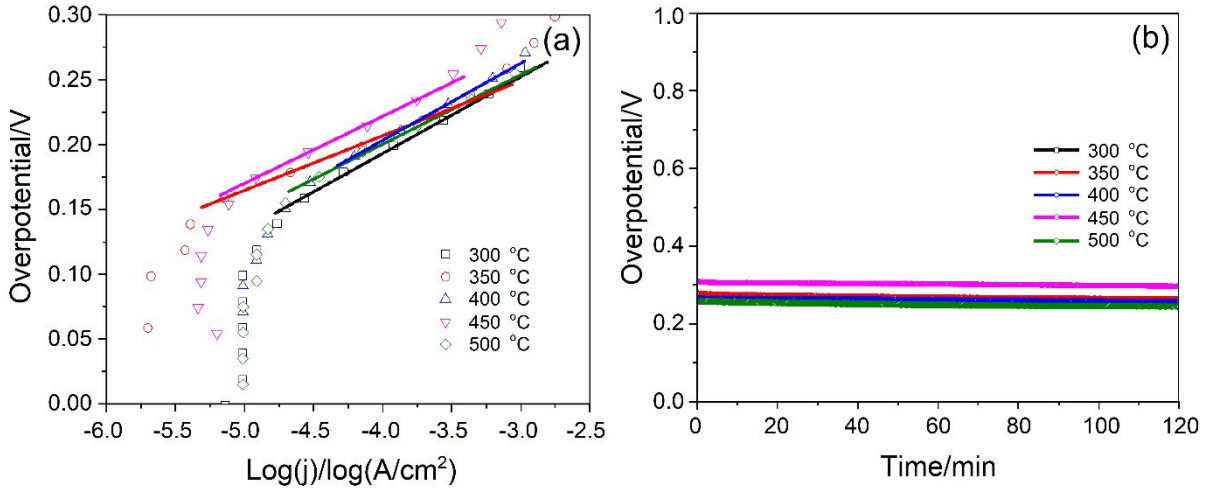

Figure S15. (a) Tafel plots, (b) CP at 1 mA/cm^2 current density for 2 hrs.

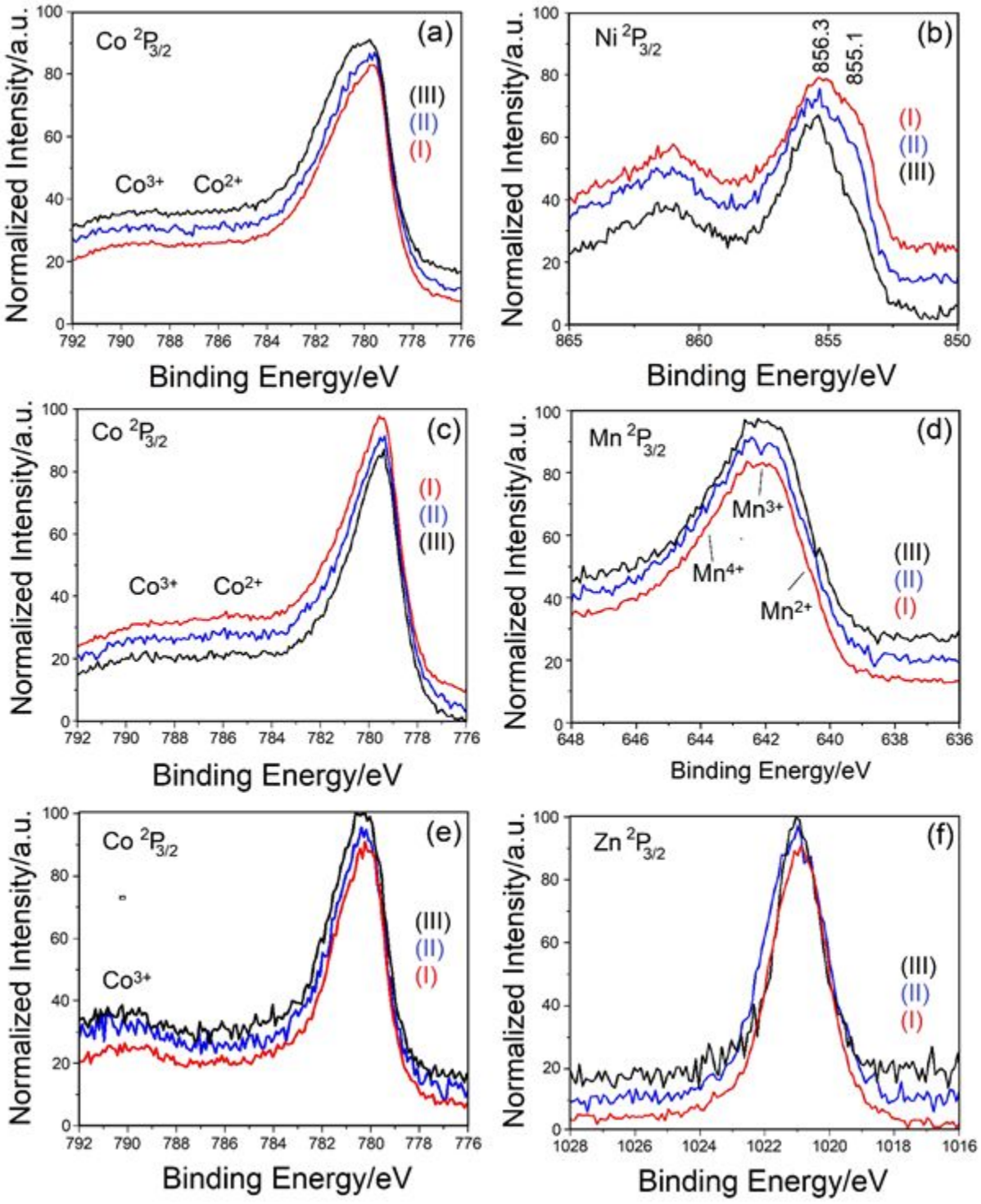

Figure S16. High resolution XPS spectra of m-$NiCo_2O_4$-10-350 (a, b), m-$MnCo_2O_4$-10-350 (c, d), and m-$ZnCo_2O_4$-10-350 (e, f). The spectra (I) FTO surface before, (II) ground sample before, and (III) ground samples after CP experiments.

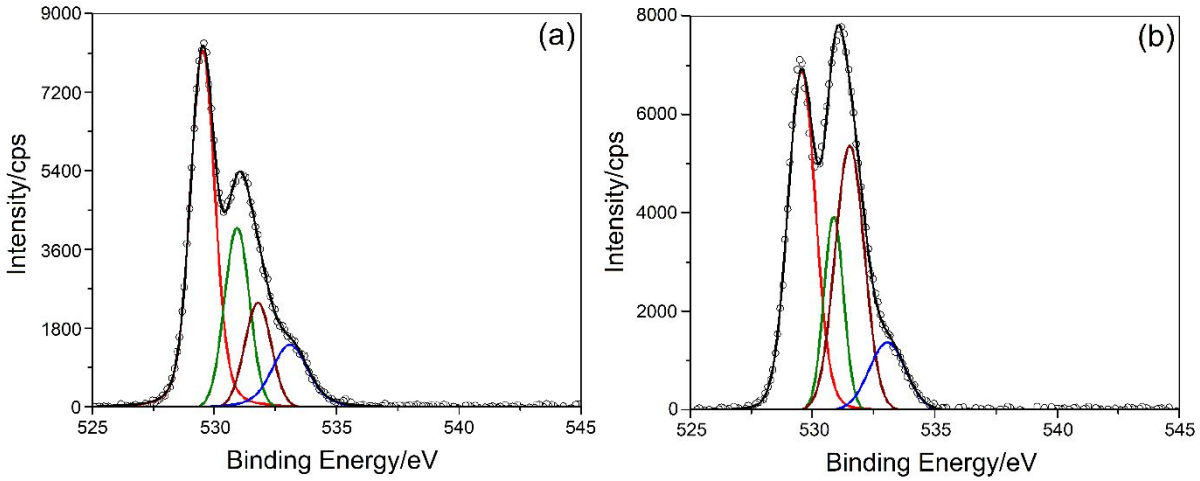

Figure S17. High resolution convoluted O 1s XPS spectra of m-$NiCo_2O_4$-10-350 electrode (a) before and (b) after CP experiments.

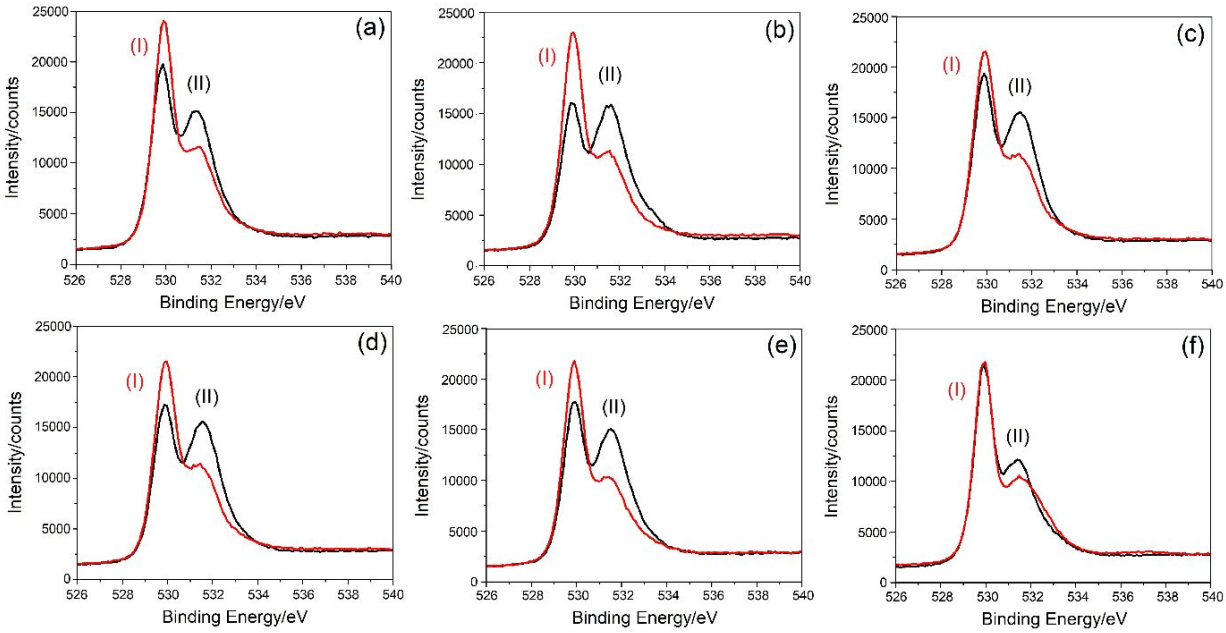

Figure S18. High resolution O 1s XPS spectra of m-$NiCo_2O_4$-10-XXX electrode (I) before and (II) after CP experiments. XXX is (a) 300 ^oC, (b) 350 ^oC, (c) 400 ^oC, (d) 450 ^oC, (e) 500 ^oC, and (f) 700 ^oC.

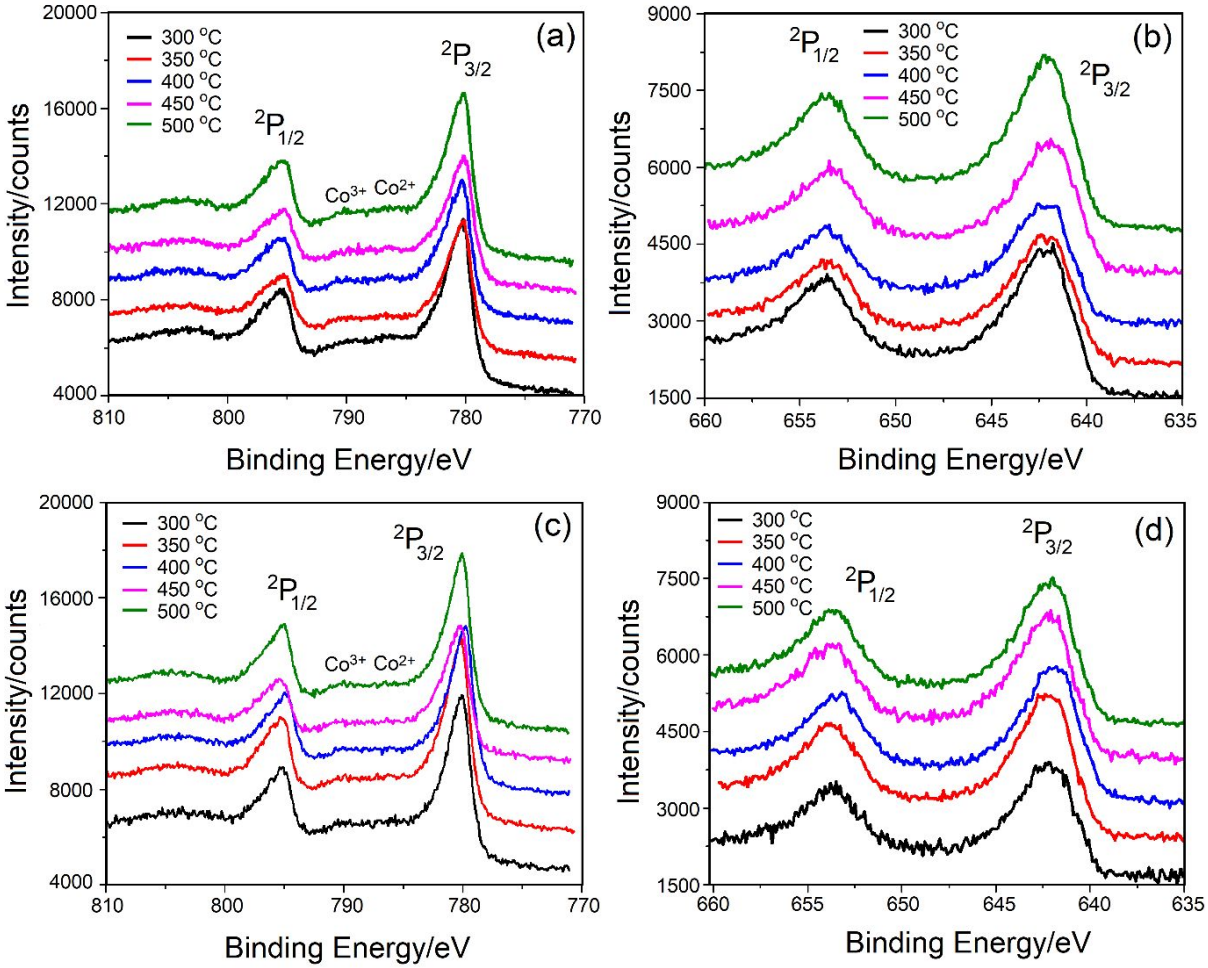

Figure S19. High resolution XPS spectra of m-$MnCo_2O_4$-10-XXX (XXX are given in the panels): Top spectra before multistep CP measurements (a) Co 2p, and (b) Mn 2p and bottom spectra after multistep CP measurements (c) Co 2p, and (d) Mn 2p regions.

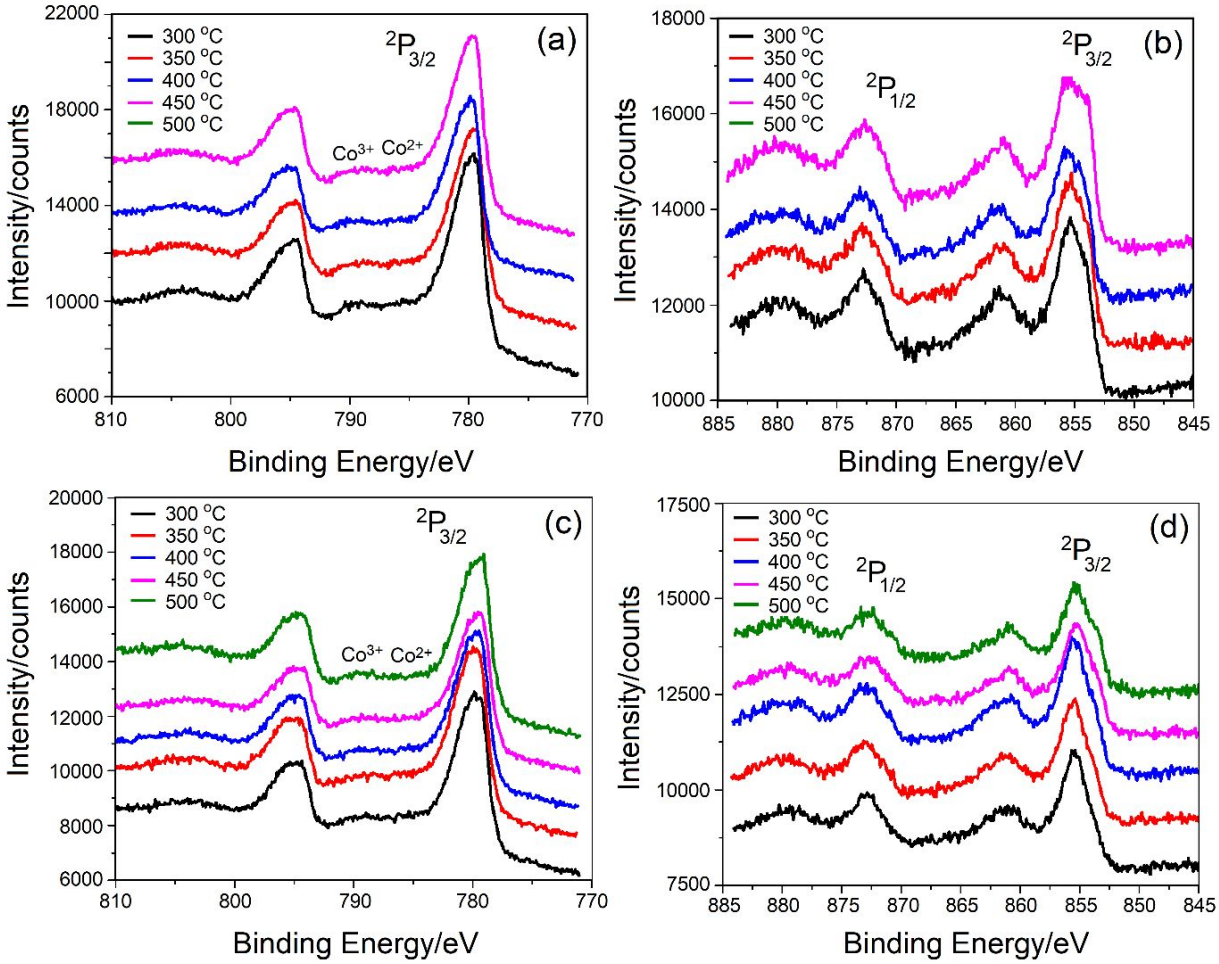

Figure S20. High resolution XPS spectra of m-$NiCo_2O_4$-10-XXX (XXX are given in the panels): Top spectra before multistep CP measurements (a) Co 2p, and (b) Ni 2p and bottom spectra after multistep CP measurements (c) Co 2p, and (d) Ni 2p regions.

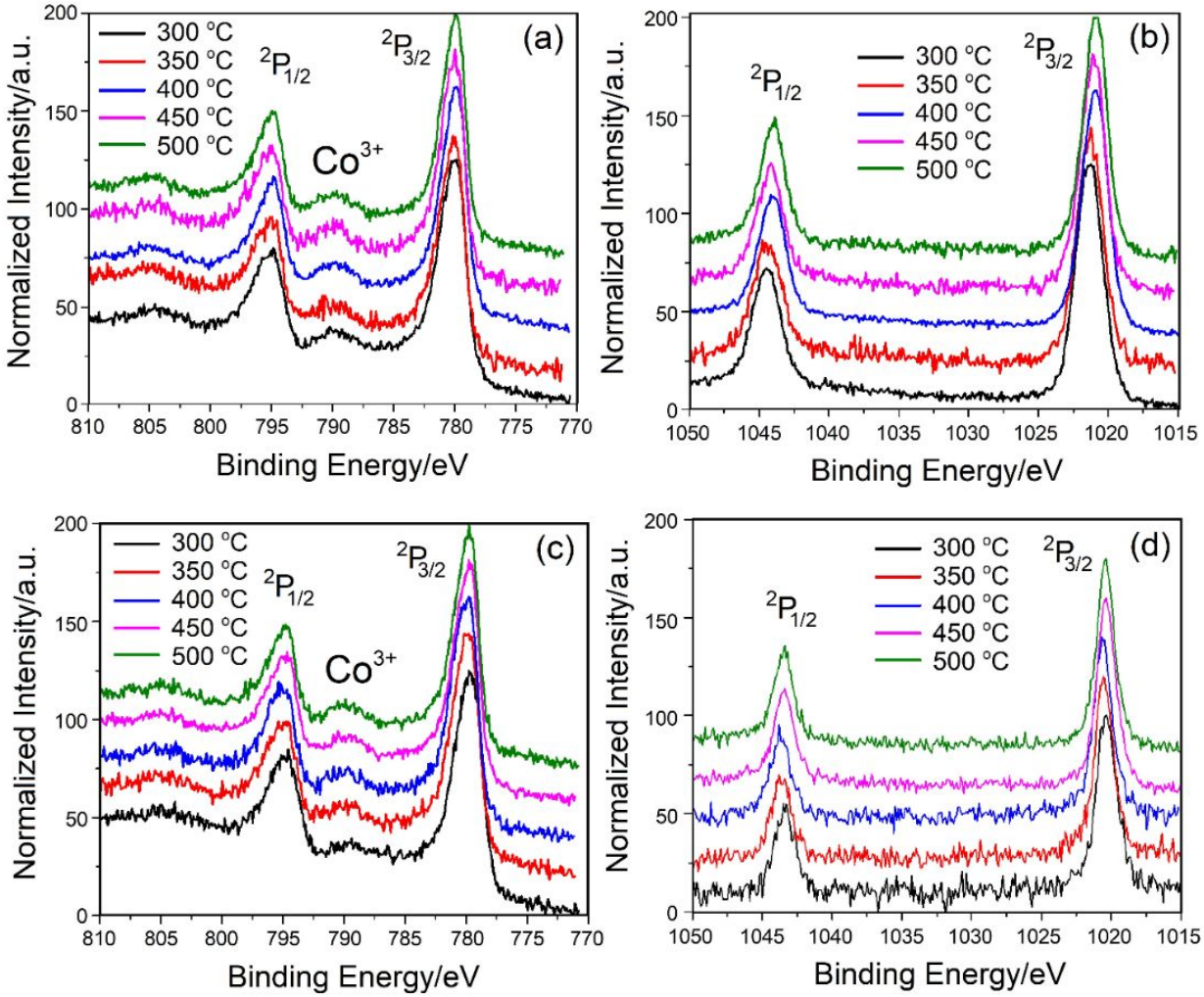

Figure S21. High resolution XPS spectra of m-$ZnCo_2O_4$-60-XXX (XXX are given in the panels): Top spectra before multistep CP measurements (a) Co 2p, and (b) Zn 2p and bottom spectra after multistep CP measurements (c) Co 2p, and (d) Zn 2p regions.

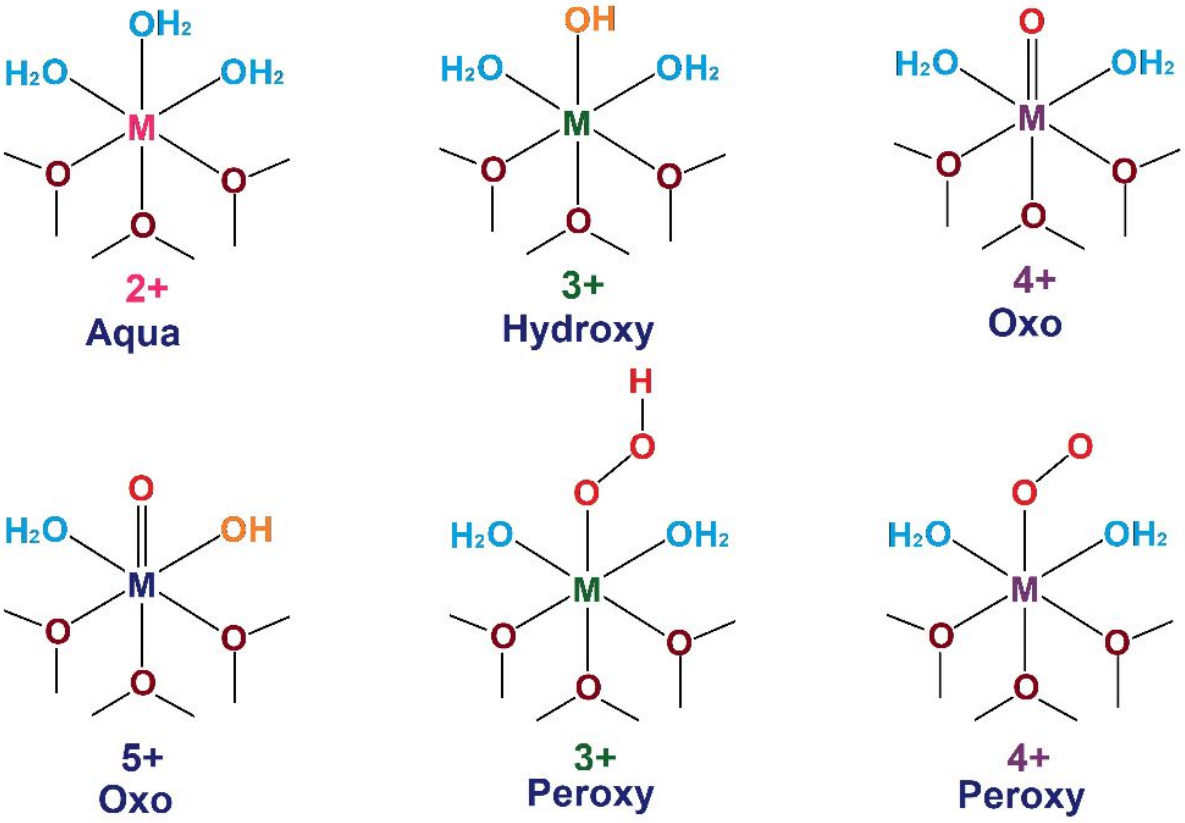

Figure S22. Structures of the likely surface species and oxidation state of the metals.